ACS APPLIED MATERIALS & INTERFACES

Research Article

www.acsami.org

Graphene/NiO Nanowires: Controllable One-Pot Synthesis and Enhanced Pseudocapacitive Behavior

Duc Tai Dam, Xin Wang, and Jong-Min Lee*

School of Chemical and Biomedical Engineering, Nanyang Technological University, Singapore 637459, Singapore

Supporting Information

ABSTRACT: In this study, we report a facile and simple approach to synthesize a composite of mesoporous NiO nanowires and graphene nanosheets for supercapacitor applications. A Ni precursor was prepared by a one-pot sol–gel method in a water/ethylene glycol mixture containing a graphene oxide. Heat treatment in air was carried out to thermally reduce the graphene oxide to graphene and to convert the Ni precursor to NiO. NiO nanowires possess a rough surface, have a diameter of around 60 nm and are homogeneously deposited on the graphene sheets. The NiO/graphene nanocomposite demonstrates superior pseudocapacitive properties (high specific capacitance, good cyclic performance, and excellent discharge rate capability) as compared to its counterparts. We postulated that this phenomenon arose from the synergistic effect of the addition of graphene as elastic conductive channels, which resulted in better charge transport and more favorable ionic diffusion.

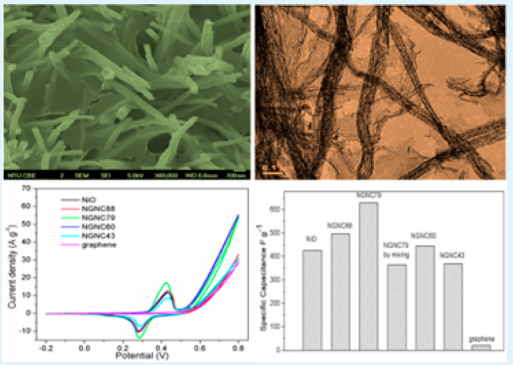

KEYWORDS: *nickel oxide, graphene, nanowire, synergistic effect, supercapacitor, sol–gel*

INTRODUCTION

Over the past decade, because of increasing environmental pollution and depletion of fossil fuels, considerable effort has been devoted to the development of clean and sustainable sources of energy.[1,2] On top of that, the latest technological advancements in the market of hybrid electric vehicles and electronic devices lead to a need for alternative energy storage devices with higher power and energy densities. In recent years, electrochemical capacitors (ECs) have drawn a great deal of attention as an alternative sustainable source of energy because of their ability to deliver higher energy density than conventional capacitors and higher power density than secondary batteries. As such, ECs are considered as intermediate energy systems between dielectric capacitors and batteries.

On the basis of the nature of charge storage mechanisms and electrode materials, electrochemical supercapacitors can be typically categorized into two main groups: electrical double-layer capacitors (EDLCs) and pseudocapacitors (redox supercapacitors). In EDLCs, conductive inert materials with high surface area are utilized to store energy by charge accumulation at the electrochemical electrode/electrolyte interface. Pseudocapacitor electrodes are made of redox materials that have reversible faradaic reactions with electrolytes on their surface. Carbonaceous materials such as activated carbon[3] and carbon nanotubes[4,5] have been commonly employed as electrode materials for EDLCs. Transition metal oxides including nickel oxide are promising candidates for the next generation of redox materials in pseudocapacitors.

Carbon nanotubes (CNTs) are considered as the most promising electrode material because of their unique structure and properties, which allows their wide applications in various fields, such as energy storage systems, sensors and catalysts.[5] In recent years, attention has gradually shifted to another hot carbon-based material because of its intriguing monolayer arrangement of carbon atoms forming a honeycomb network. Since its discovery in 2004, graphene and its derivatives have been regarded as two-dimensional unrolled carbon nanotubes with bright future. In the past decade, tremendous effort has been devoted to studying interesting characteristics of graphene-based materials, as well as, exploring different synthesis pathways. Despite the fact that graphene can be prepared by multiple approaches, it is still commonly synthesized via production of graphene oxide (GO) achieved by Hummers method. This technique allows mass production of graphene for large-scale applications. The reduction from GO to graphene is mainly achieved by a chemical route employing a large amount of concentrated reducing agents, such as hydrazine,[6] hydroquinone,[7] and sodium borohydride.[8] Nonetheless, this approach is preferred mostly when reduced graphene oxide (rGO) is required because of the toxic nature of the reducing agent. Therefore, limited usage of the reducer is highly desired and an alternative reduction pathway must be explored to produce graphene in bulk. Surprisingly, in this study, we found that rGO prepared by chemical pathways can

Received: February 18, 2014
Accepted: May 9, 2014
Published: May 20, 2014

   dx.doi.org/10.1021/am500700x | ACS Appl. Mater. Interfaces 2014, 6, 8246–8256

sustain and completely reduce to graphene through calcination at temperatures up to 400 °C in air. This technique opens up the opportunity to mass produce graphene and incorporate graphene in hybrid structures with other metal oxides, of which preparation requires heat treatment in air at elevated temperatures.

Among transition metal oxides (TMOs), ruthenium oxide (RuO_2) is still considered as the most common active material for fabrication of supercapacitor electrodes, largely because of its high capacitive activity. However, limited resources and high-cost create barriers to its wide commercialization. As a result, it is imperative to develop alternative redox materials to replace ruthenium oxide.[9,10] Nickel oxide (NiO) is of particular interest as one viable candidate because of its abundancy, cost effectiveness, and well-defined electrochemical properties. From our point of view, electrochemical performance of a NiO nanostructure depends on its surface area, particles size, crystal structure, and morphology. Basically, mesoporous nanostructures have been fabricated to develop supercapacitor electrodes with a high surface area.

Nanocomposite and nanoarchitecture electrodes in which metal oxides/hydroxides were integrated with carbonaceous materials have been intensively investigated for supercapacitors and lithium-ion batteries.[11−13] Inspired by their work, in this study, we demonstrate an approach that combines advantageous characteristics of both graphene and mesoporous nickel oxide in graphene/NiO nanowire nanocomposite. A one-pot synthesis of rGO/Nickel oxalate nanowire was carried out by a sol−gel technique followed by a heat treatment at a high temperature to prepare the graphene/NiO nanowire composite. To the best of our knowledge, this kind of nanostructure has not been studied or reported elsewhere. We also performed investigation on electrochemical properties of an as-prepared hybrid supercapacitor electrode with carbon paper as current collector. The effect of graphene content in the composite electrode on pseudocapacitive behavior was also thoroughly studied to determine an optimal ratio and provide insight into the synergistic effect of both counterparts.

EXPERIMENTAL SECTION

Preparation of Graphene Oxide (GO). GO was prepared through exfoliation of a chemically oxidized flake graphite powder by modified the Hummers method.[14] In detail, commercial graphite (1 g, <20 μm, Sigma-Aldrich) was added into concentrated H_2SO_4 (98%, 23 mL) in a 250 mL round-bottom flask under stirring in an ice bath. One gram of $NaNO_3$ and 3 g of $KMnO_4$ were gradually put into the dispersion under intensive stirring for 30 min at an ice bath temperature until a purple-green mixture was obtained. This suspension was then transferred to a 35 °C water bath and magnetically stirred for 24 h to achieve a dark brown color paste. Subsequently, 20 mL of DI water was added to the mixture and an oxidation reaction was allowed to proceed for another 96 h. The reaction was terminated by addition of a good amount of DI water and 30% H_2O_2 solution (3 mL). The mixture was subjected to centrifugation and suspension in 5% HCl solution and mechanical agitation to completely remove metal ions. The product was then washed with a copious amount of DI water to adjust the pH to around 6. The as-obtained graphite oxide was dispersed in DI water and exfoliated by a tip sonicator to prepare the GO dispersion.

Sol−Gel Synthesis of rGO/Nickel Oxalate Nanowire and Graphene/NiO Nanowire Composites. Chemically derived NiO/graphene nanocomposites (NGNCs) with different feed ratios were prepared. The composites were labeled as NGNCpercentage in which the percentage indicates the content/weight percentage of NiO determined by TGA analysis. In a representative synthesis of $NGNC_{79}$, 0.015 g of exfoliated GO was dispersed in a mixture of 15 mL of DI water and 35 mL of ethylene glycol (EG, anhydrous, Sigma-Aldrich) by sonication for 1 h to ensure uniformity in suspension. Subsequently, 0.118 g of $NiCl_6.6H_2O$ (Sigma-Aldrich) was dissolved into the mixture followed by the addition of 0.5 mL of 1 M of an aqueous oxalic acid solution. The mixture was then transferred into a 100 mL round-bottom flask and heated to 120 °C in a silicon oil bath under a reflux condition with vigorous stirring. After refluxing for 2 h, a 100 μL hydrazine solution (N_2H_4, 35%, Sigma-Aldrich) was rapidly added to boiling solution. The mixture was maintained at this temperature for another 22 h and allowed to cool to room temperature. The blackish precipitate was then centrifuged, washed repeatedly with a copious amount of absolute ethanol and DI water, and finally freeze-dried for 24 h. Finally, the as-prepared product was calcined in the air at 400 °C for 1 h to acquire the graphene/NiO nanowire composite. For comparison studies, pure graphene, pure NiO nanowire and graphene/NiO nanowire composites of different ratios were also prepared.

Characterization. Powder X-ray diffraction (XRD) analyses were performed by a Bruker D8 Advance X-ray Diffractometer equipped with Cu Kα radiation (λ = 0.15406 nm) in the ranges from 10 to 70°. Raman measurements were also carried out by a Renishaw inVia Raman microscope equipped with a charge couple device (CCD) detector to analyze chemical bonding states of the surface. X-ray photoelectron microscopy (XPS) characterization was performed by a VG ESCALAB 220I-XL system. Morphologies of as-obtained products were studied by a field emission scanning electron microscopy (JEOL-JSM-6700F microscope) operated at 5 kV. Structure analyses were conducted by a transmission electron microscopy (TEM, JEOL 2010) at 300 kV. Thermogravimetric analysis (TGA) was performed with the temperature ramping rate of 10 °C min^{-1} by Diamond TG/DTA (PerkinElmer). The nitrogen adsorption−desorption spectra of the samples were obtained by Brunauer−Emmett−Teller (BET) measurements using Autosorb 6B at −196 °C. The FTIR spectra were recorded by Spectrum One with ATR (PerkinElmer) and dry KBr was used as background material.

Electrochemical Measurement. The electrochemical measurements of the as-prepared electrodes were carried out by CHI660d electrochemical workstation in a three-electrode cell configuration and in a 6 M KOH electrolyte. The working electrodes were prepared by mixing the as-synthesized graphene/NiO nanowire composite (75 wt %) with acetylene black (20 wt %), and poly(tetrafluoroethylene) (5 wt %). The obtained mixture was dispersed in ethanol. The mixture was then dropped onto carbon paper and dried at 70 °C in a vacuum oven overnight to remove the solvent. The mass of loading was controlled in the range of 1.0−1.2 mg over an area of 1 cm^2 of carbon paper. The reference electrode and counter electrode were a standard Ag/AgCl electrode and a platinum plate (Pt), respectively. The electrochemical performances of the as-synthesized products were evaluated by cyclic voltammetry (CV) in potential ranges from −0.2−0.8 V and specific capacitance was quantified by chronopotential charge/discharge measurement potential windows of 0−0.5 V, based on the following equation[15]

$$C = \frac{I\Delta t}{m\Delta V} \tag{1}$$

where C is the specific capacitance (F g^{-1}), I is the current (A), Δt is the discharge time (s), m is the mass of active composite material (g), and ΔV is the potential window (V).

The energy density (E) and power density (P) were determined from the discharge curves using the following eqs 2 and 3, respectively.[16]

$$E = \frac{1}{2}C\Delta V^2 \tag{2}$$

$$P = \frac{E}{\Delta t} \tag{3}$$

Electrochemical impedance analysis was also conducted by Autolab PGSTAT302 potentiostat.

RESULTS AND DISCUSSION

The process of preparation of rGO/$Ni_2C_2O_4{\cdot}2H_2O$ and graphene/NiO nanocomposites is illustrated in Figure 1.

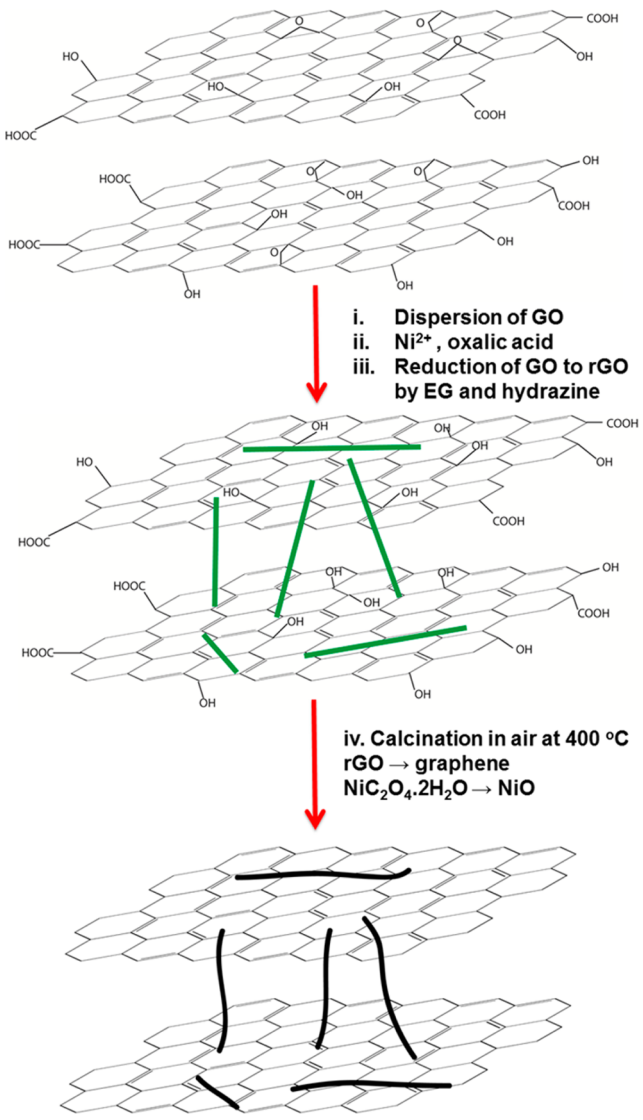

Figure 1. Schematic representation of the fabrication process of graphene/NiO nanowire composite. (i) Dispersion of GO in mixture of water and ethylene glycol (EG). (ii) Nucleation and formation of NiC_2O_4 nanowire. (iii) Reduction of GO to rGO by EG and hydrazine solution. (iv) Calcination in air resulting in conversion of NiC_2O_4 to NiO and complete reduction of rGO to graphene.

Because of functional groups such as carboxyl, hydroxyl, and epoxyl groups bonded to carbon on the surface, GO possesses a strong hydrophilic nature. This facilitated the absorption of Ni^{2+} species and anisotropic growth of $Ni_2C_2O_4$ nanowires. Ethylene glycol and N_2H_4 also helped in reducing GO to rGO. $Ni_2C_2O_4$ was then thermally converted to NiO and rGO was completely reduced to graphene by calcination in a muffle furnace. This approach is expected to result in a strong interaction between the nanowires and the graphene sheets, which potentially leads to enhanced charge transport. More importantly, the addition of graphene can help in preventing the agglomeration of the pristine NiO nanowires commonly encountered in sol−gel preparations. Therefore, the presence of graphene could improve the electrolyte diffusion at the electrode/electrolyte interface.

Thermal analysis was first performed to investigate the thermal stability of rGO and the precursors with different nickel contents obtained from the sol−gel method. Three typical TGA curves of rGO, nickel oxalate dihydrate, and rGO/$Ni_2C_2O_4{\cdot}2H_2O$ or a NGNC79 precursor in air are presented in Figure 2. From the thermogravimetric analysis of rGO reduced by combined ethylene glycol and hydrazine, mass loss starts at around 200 °C, because of the decomposition of the remaining functional groups. The complete combustion of graphene was attained at around 550 °C. Both $Ni_2C_2O_4{\cdot}2H_2O$ and rGO/$Ni_2C_2O_4{\cdot}2H_2O$ exhibit initial weight loss at around 200 °C, which is probably due to the removal of the adsorbed moisture and dehydration. At a higher temperature of 320 °C, the organic precursors start to decompose which leads to a formation of NiO as a final product. Decomposition of $Ni_2C_2O_4{\cdot}2H_2O$ is complete at 350 °C and full conversion to NiO is achieved. The NiO product is stable from 350 to 800 °C without any considerable weight loss/gain. On the other hand, due to the presence of graphene in the nanowire network, rGO/$Ni_2C_2O_4{\cdot}2H_2O$ continued to decompose in the temperature ranges from 350 to 450 °C. In this study, all precursors were calcined in air at 400 °C. Hence, the difference between weight at 400 °C and the final weight derived from TGA curves was referred as graphene content in graphene/NiO (NGNC) products and utilized to estimate the weight ratio. The TGA curves of NGNC88, NGNC60, and NGNC43 precursors were also prepared and shown in Figure S1 (see the Supporting Information).

As an attempt to gain insight into the as-synthesized precursor and final product, XRD and Raman measurements were performed. Powder X-ray diffraction technique is a reliable technique to determine crystal structure of samples. The diffraction patterns of rGO/$Ni_2C_2O_4{\cdot}2H_2O$ hybrid structures with different feeding ratios were identical. Representative XRD patterns of the precursor of NGNC79 and the final product upon completion of the thermal treatment are shown in Figure 3a. Comparing the XRD results of the as-prepared precursor with the reference database allows us to identify the product of the sol−gel synthesis to be $Ni_2C_2O_4{\cdot}2H_2O$ (JCPDS 25−0581). $Ni_2C_2O_4{\cdot}2H_2O$ crystallizes in a monoclinic system of which a unit cell is composed of four molecules and the metal oxalate layers are stabilized by hydrogen bonds with H_2O ligands. The peak with the highest intensity at 2θ = 18.8° can be assigned to the (−202) plane and interplanar spacing of 0.47 nm. The other peaks at 2θ = 22.6, 24.9, 30.3, 33.9, 35.4, 37.4, 42.1, 43.7, 47.7, and 48.7° can be attributed to (002), (−112), (−402), (−113), (021), (−204), (−513), (−223), (−604), and (023) reflections, repetitively. Even though the sol−gel process did not result in formation of NiO directly, upon calcination at a high temperature, $Ni_2C_2O_4{\cdot}2H_2O$ was thermally converted to NiO. The nickel oxide crystal structure was confirmed by XRD analysis (JCPDS 47−1049). The diffraction spectrum of the NiO show reflection peaks at 2θ = 37.2, 43.3, and 62.9° which correspond to the (111), (200), and (220) crystal planes. On top of that, no peaks other than those of the NiO were detected, suggesting a complete conversion to nickel oxide without any byproduct. No peaks associated with graphene oxide and reduced graphene oxide were detected in the XRD result of the composite materials due to insufficient content, disordered stacking and uniform dispersion of the graphene sheets, which has been commonly reported in many

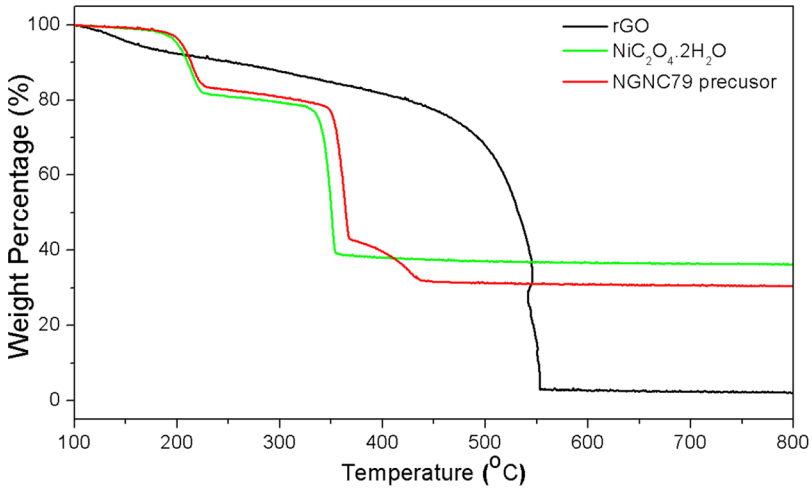

Figure 2. TGA plot of rGO, nickel oxalate dihydrate, and precursor of NGNC79 (NiO:graphene = 79 wt %:21 wt %).

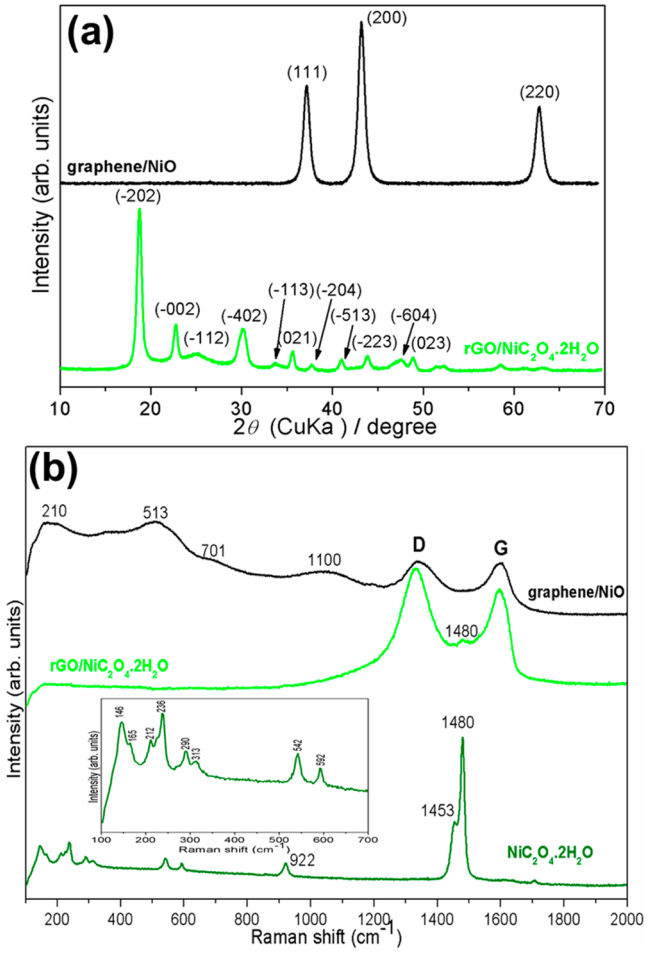

Figure 3. (a) XRD patterns of representative rGO/NiC_2O_4·$2H_2O$ and graphene/NiO. (b) Room-temperature Raman spectra of NiC_2O_4·$2H_2O$, representative rGO/NiC_2O_4·$2H_2O$, and graphene/NiO in the range of 100−2000 cm^{-1} (the inset is the enlarged view of NiC_2O_4·$2H_2O$ spectrum in the range of 100−700 cm^{-1}).

studies.[17,18] Therefore, to confirm the presence of graphene in the composite, Raman and X-ray photoelectron spectroscopy measurements were subsequently performed.

The XRD measurement was also performed on GO which exhibits a highly intensive peak at around 2θ = 10.3° and no graphite peaks were observed, suggesting a complete oxidation of graphite (Figure S2a, see the Supporting Information). XRD patterns of rGO obtained by chemical reduction and graphene prepared by thermal decomposition were relatively identical and hence, only one representative XRD spectrum was presented in Figure S2b (see the Supporting Information). Graphene demonstrates a broad peak at 2θ = 25−27.5°, implying the disordered stacking of graphene sheets. The stacking phenomenon is commonly encountered with nanosheet structures and can be observed in a TEM image of rGO at a high magnification showed in Figure S3 (see the Supporting Information). On top of that, a close comparison between diffraction spectrum of $Ni_2C_2O_4$·$2H_2O$ (Figure S2c, see the Supporting Information) and that of rGO/$Ni_2C_2O_4$·$2H_2O$ allow us to see peak broadening effects at around 2θ = 25°. This is likely due to the overlapping between (−112) peak of $Ni_2C_2O_4$·$2H_2O$ and broad (002) peak of rGO.

Figure 3b shows the Raman spectra of pure $Ni_2C_2O_4$·$2H_2O$ nanowire, the rGO/$Ni_2C_2O_4$·$2H_2O$ composite, and the graphene/NiO obtained by heat treatment. In the spectrum of the $Ni_2C_2O_4$·$2H_2O$ nanowire, three shoulder bands at 146,165, and 212 cm^{-1} are still unknown up to now. The peaks at 236 and 290 cm^{-1} can be assigned to a Ni−O symmetric stretching mode. The bands at 313, 592 cm^{-1} are attributed to a Ni−O ring stretching mode. The 542 cm^{-1} peak represents the ring deformation mode in the oxalate anion. The peaks at 922, 1453, and 1480 cm^{-1} demonstrate C−C or C−O stretching modes.[19] It is surprising to note that only the most intensive peak at 1480 cm^{-1} can be detected in the Raman spectrum of rGO/$Ni_2C_2O_4$·$2H_2O$. On the other hand, two signature peaks of rGO can be seen and labeled as D and G bands, which are classified as breathing modes of κ-point phonons of A_{1g} symmetry and E_{2g} phonon of C sp^2 atoms, respectively. The successful conversion of nickel oxalate to nickel oxide was also confirmed by the Raman spectrum of graphene/NiO. The first two peaks centralized at 210 and 513 cm^{-1} can be assigned to a Ni−O lattice vibration mode.[20,21] The next two bands are two-phonon (2P) modes (2TO mode at 701 and 2LO mode at 1100 cm^{-1}) of nickel oxide.[22] On the other hand, the ratio of intensity of two bands (i.e., I_D/I_G) generally decreased after heat treatment, implying a high efficiency of thermal reduction.[23]

To determine the chemical composition of the NiO/graphene composite, X-ray photoelectron spectroscopy (XPS)

dx.doi.org/10.1021/am500700x | ACS Appl. Mater. Interfaces 2014, 6, 8246−8256

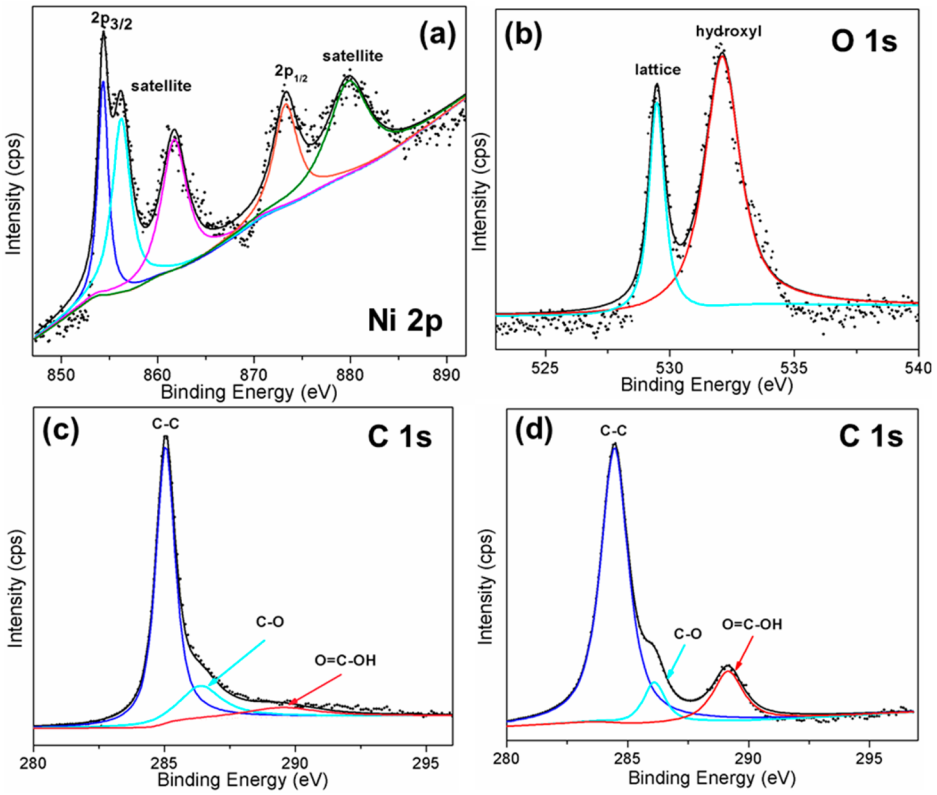

Figure 4. XPS spectrum (a) Ni 2p, (b) O 1s, and (c) C 1s of NiO/graphene composite and (d) C 1s of rGO/$NiC_2O_4{\cdot}2H_2O$ composite.

characterization was conducted in the binding energy region from 0 to 1100 eV (Figure 4). The peaks were fitted as close to the data points as possible in order to retain the intrinsic nature and reliability of data set. The Ni $2p_{3/2}$ and Ni $2p_{1/2}$ spectra are presented in Figure 4a and depict 5 discernible peaks: $2p_{3/2}$ (854.4 eV) and its satellites (856.1 and 861.7 eV), $2p_{1/2}$ (873.4 eV) and its satellite (879.8 eV), all of which can be attributed to the presence of NiO. The O 1s spectrum of NiO (Figure 4b) is composed of two main peaks at 529.5 and 532.3 eV resulting from the lattice oxygen and the surface hydroxyl group, respectively.[24,25] Hydroxylation is a ubiquitous phenomenon commonly encountered in metal oxide materials. And this phenomenon is also observed in this study. This is largely due to the prolonged exposure of the sample to an ambient environment. The peak at 532.3 eV indicates the presence of retained oxygen-containing groups such as −OH and −COOH linked to the carbon atoms of graphene. On top of that, moisture in air can also be adsorbed to the NiO surface and give rise to this peak. The C 1s spectrum (Figure 4c) exhibits three peaks at 284.8, 286.4, and 289.4 eV corresponding to graphitic carbon in graphene, C−O (epoxy) and COOH groups. On the other hand, an XPS measurement can also provide a clear demonstration of thermal reduction of reduced graphene oxide to graphene at 400 °C. The C 1s spectra of rGO/$NiC_2O_4{\cdot}2H_2O$ are also displayed in Figure 4d. Because of the heat treatment at an elevated temperature, the intensities of C 1s peaks of carbon binding to oxygen (i.e., epoxy and carboxylic) decreases considerably, indicating that most oxygen groups were removed. The effect of thermal reduction was also further confirmed by a result of an FTIR analysis shown in Figure S4 (see the Supporting Information).

To study the structure of the rGO/$Ni_2C_2O_4{\cdot}2H_2O$ composite, we first examined its morphology and crystal structure. Figures 5a and 5b are representative FESEM images showing the network of $Ni_2C_2O_4$ nanowires interlaced with rGO sheets. During characterization, it was observed that nanowires with lengths up to a micrometer scale entangled with one another to form nanobundles. The surfaces of rGO sheets are partially covered by interconnected nanowires. As shown in Figure 5c, the surface of the nickel oxalate nanowire is smooth with a relatively uniform diameter of around 60 nm. Similar observations can also be confirmed by a TEM image at a low magnification (Figure 5d). It is worth noting that the rGO sheets curl and wrap around bundle of nanowire, as revealed in Figure 5e. HRTEM image of NiC_2O_4 suggests that nanowire is polycrystalline with representative (−314), (−604), and (−202) crystallographic planes.

EFTEM mapping of the rGO/$Ni_2C_2O_4{\cdot}2H_2O$ was also performed to investigate the elemental distribution within composite structure and spatial distribution of oxygen and nickel on the surface of the graphene (see Figure S5 in the Supporting Information). O is likely to be evenly incorporated with Ni along the nanowires. In addition, there is a small amount of an oxygen element on the rGO sheets, which could originate from unremoved functional groups. Carbon existence can be observed everywhere because of the carbonaceous nature of rGO.

The morphology and the crystal structure of the final product, the graphene/NiO nanowire, were also investigated to study the effects of heat treatment. Wire-like morphology is retained and the distribution of nanowire on the graphene becomes more uniform upon the heat treatment, as shown in the FESEM images (Figure 6a−c). This is likely due to the partial decomposition of the graphene oxide by calcination at high temperatures, which lowers the graphene content in the composite. On top of that, the heat treatment at elevated

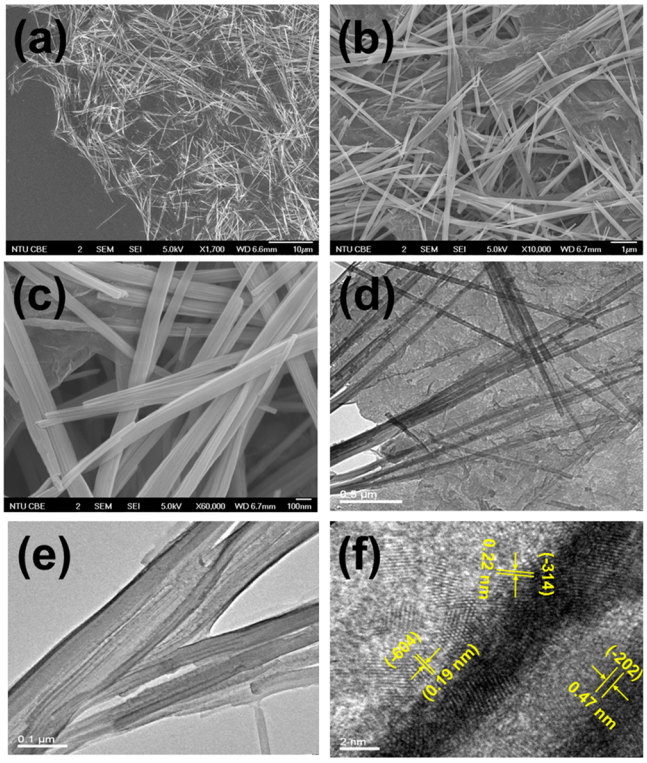

Figure 5. (a–c) FESEM images of rGO/NiC_2O_4. $2H_2O$ composite at different magnifications. (d) High-magnification TEM image of rGO/NiC_2O_4. $2H_2O$. (e) TEM image of NiC_2O_4 nanowire bundle wrapped by rGO sheets. (f) HRTEM image of NiC_2O_4 nanowire.

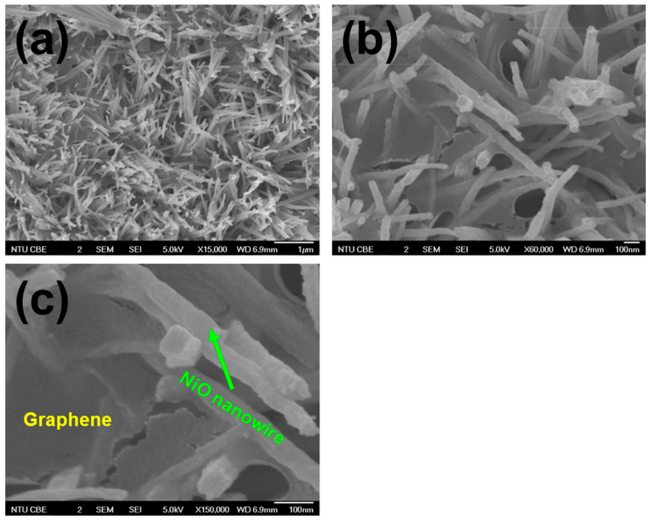

Figure 6. .(a–c) FESEM images at different magnifications of graphene/NiO nanowire composite prepared by calcination precursor at 400 °C for 3 h.

temperatures is known to help in enhancing crystallinity of metal oxide and lead to rearrangement of nanowire network, all of which result in more uniform distribution of nanowire on the graphene surface.

Low-magnification TEM images of the hybrid structure (Figure 7a) also allow us to confirm successful synthesis. It is interesting to note that the graphene sheets and NiO nanowires are partially broken, which is largely due to a rapid thermal expansion and shrinkage (Figure 7b). Instead of being smooth like the surface of the precursor nanowire, the surface of NiO

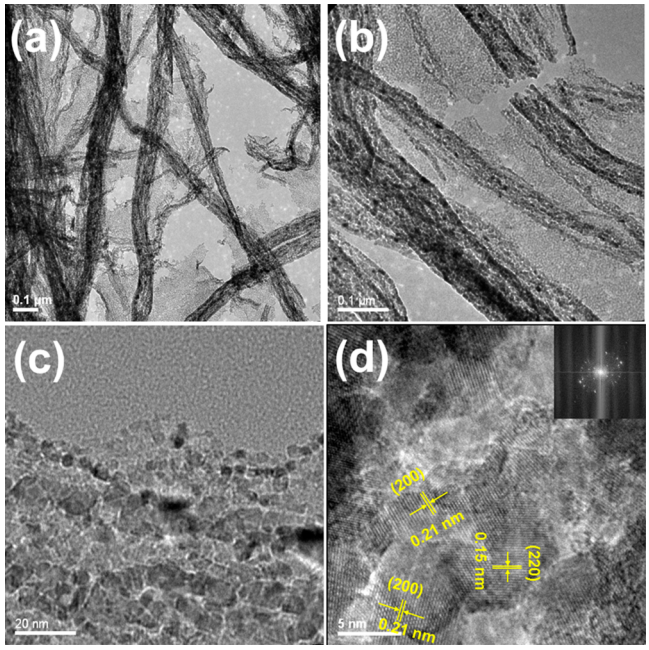

Figure 7. TEM images of graphene/NiO nanowire composite prepared by calcination precursor at 400 °C for 3 h. (a, b) low magnification TEM image of graphene and NiO nanowire network. (c) TEM image of typical NiO nanowire composed of primary nanoparticles. (d) HRTEM image of polycrystalline NiO nanowire.

nanowire is rough and consisted of many primary particles (Figure 7c). On the basis of the lattice-resolved HRTEM image (Figure 7d), NiO is also polycrystalline with mainly (200) and (220) planes of which the interplanar distance are estimated to be 0.21 and 0.15 nm, respectively.

Cyclic voltammetry (CV) and chronopotentiometry are reliable techniques to measure electrochemical properties and quantify specific capacitance. The pseudocapacitance of a NiO-based electrode can be elaborated by following faradaic reactions

$$NiO + OH^- \leftrightarrow NiOOH + e^- \quad (4)$$

In this study, to determine the optimal ratio of NiO:graphene, we performed cyclic voltammetry measurements on all graphene/NiO nanowire electrodes, with a NiO content ranging from 100 wt % to 0 wt %. The results are shown in Figure 8. Figure 8a presents the CV curves of all the electrodes in a 6 M KOH electrolyte at a scan rate of 5 mV s^{-1}. Pairs of oxidation/reduction peaks can be clearly observed in all the CV curves of any NiO-based electrodes, indicating a capacitive characteristic. The anodic peaks observed at around 0.43 V arise from the oxidation of the NiO to NiOOH. The cathodic peaks at around 0.3 V is attributed to the reverse process shown in the redox reaction 4. It is noteworthy that the potential separation between the peaks remains relatively the same and is independent of the NiO content variation. On the other hand, the CV curve of the graphene resembles the ideal rectangular shape of EDLCs. It was observed that the area under CV curve of NGNC79 is the highest, indicating the largest capacitance. As an attempt to highlight the merit of the synergistic effect in composite material, the CV of $NGNC79_{\text{by mixing}}$ (graphene/NiO nanowire electrode obtained by mixing counterparts at the same ratio as NGNC79 prepared by the one-pot sol–gel approach) was also measured and included in Figure 8b. It is interesting to note that the area under the curve of

dx.doi.org/10.1021/am500700x | ACS Appl. Mater. Interfaces 2014, 6, 8246–8256

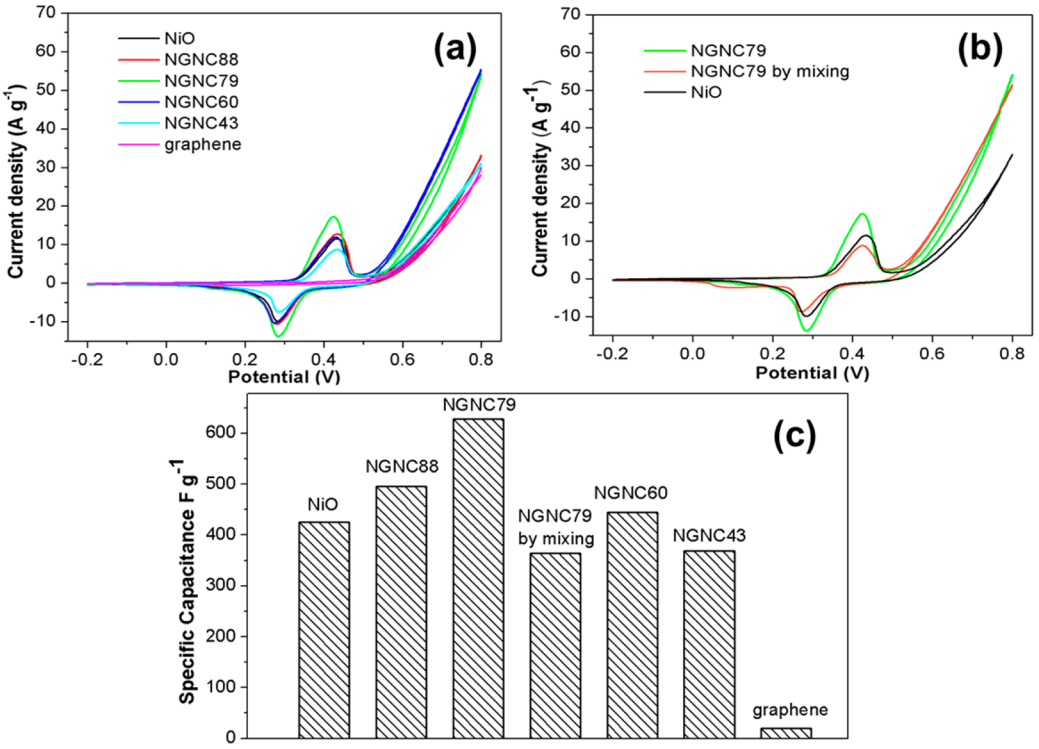

Figure 8. (a) CVs of NiO, NGNC88, NGNC79, NGNC60, NGNC43, rGO at 5 mV s^{-1}. (b) CVs of NiO, NGNC79, and graphene/NiO nanowire (21 wt %:79 wt %) obtained by mixing of counterparts at 5 mV s^{-1}. (c) Plot of specific capacitance of electrode with different NiO content at current density of 1 A g^{-1}.

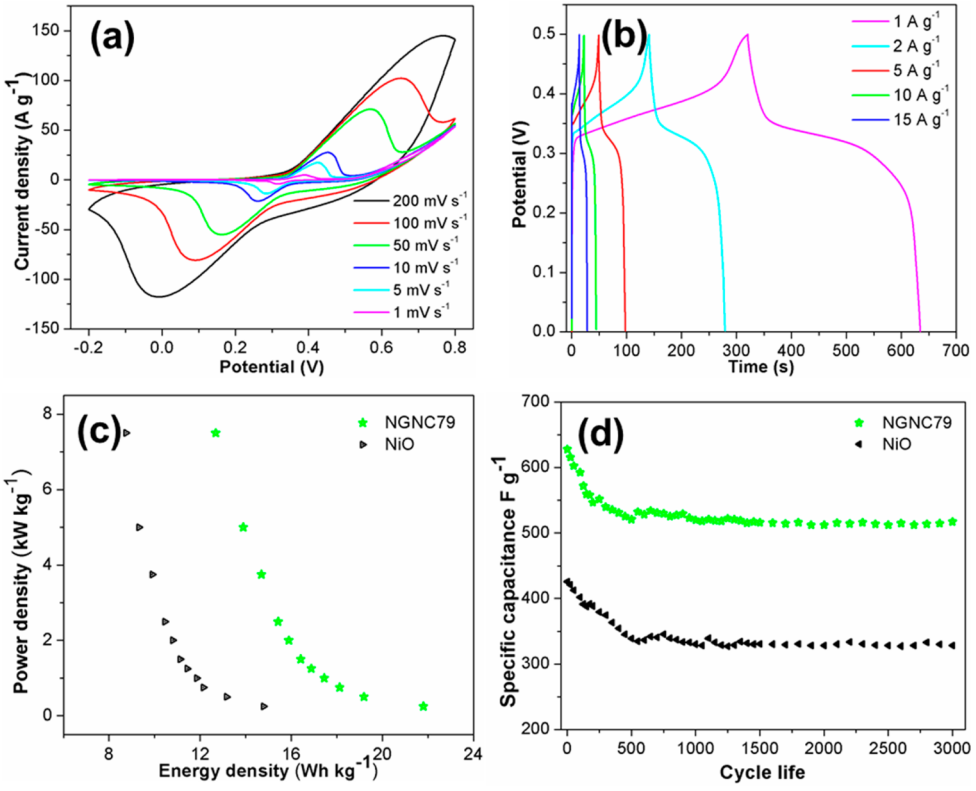

Figure 9. (a) CVs at different scan rates of NGNC79. (b) Charge/discharge plots of NGNC79 at different current densities in potential window of 0−0.5 V. (c) Ragone plot (power density vs energy density) of graphene/NiO nanowire and pure NiO nanowire electrodes derived from the charge/discharge curves at different current densities. (d) Cycle life of graphene/NiO nanowire and pure NiO nanowire electrodes at current density of 1 A g^{-1} for 3000 cycles.

dx.doi.org/10.1021/am500700x | ACS Appl. Mater. Interfaces 2014, 6, 8246−8256

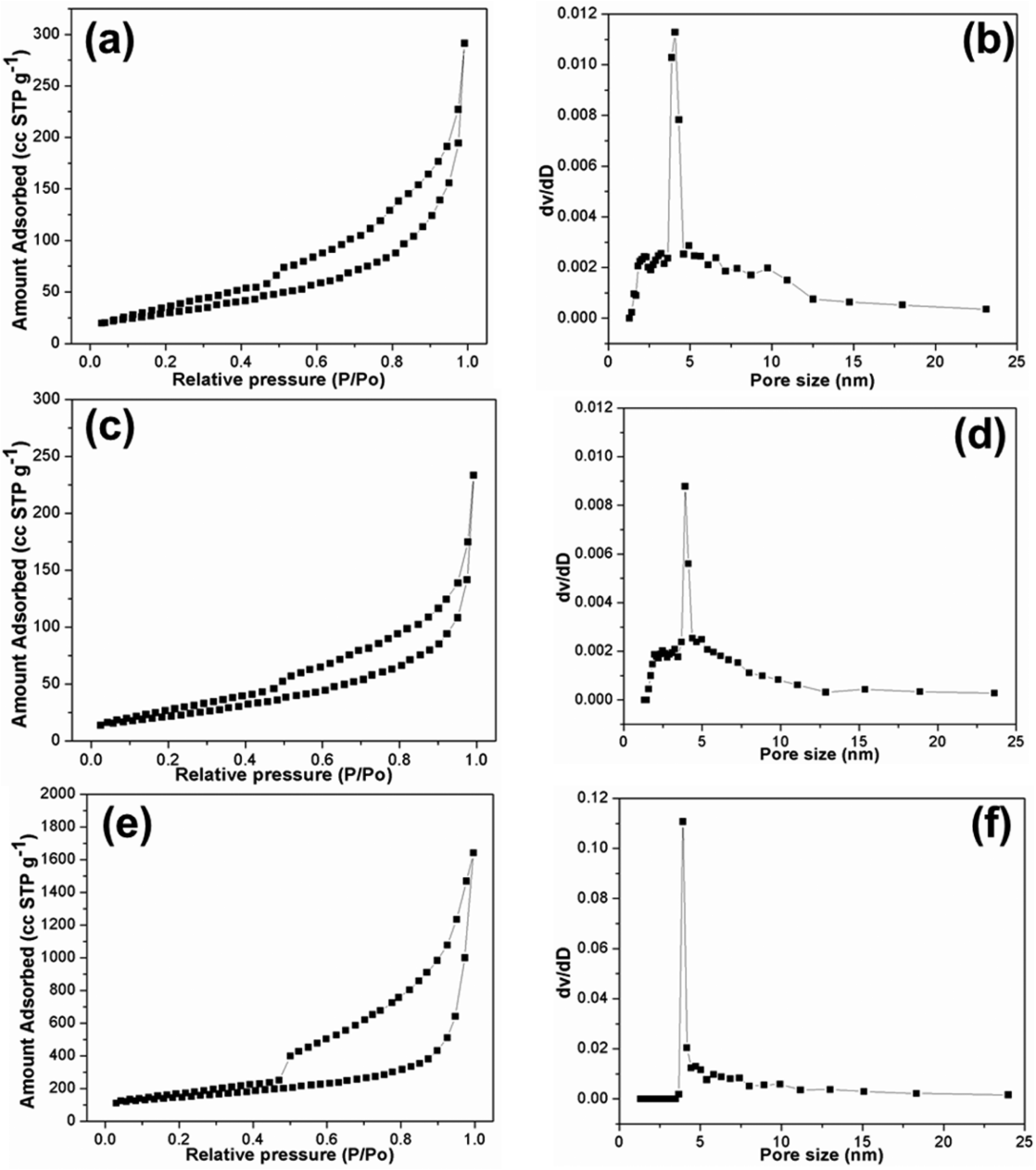

Figure 10. (a, c, e) Nitrogen adsorption−desorption isotherms of NGNC79, NiO nanowire, and graphene powder samples. (b, d, f) Pore size distribution of NGNC79, NiO nanowire, and graphene.

$NGNC79_{by\ mixing}$ is noticeably smaller than those of the NGNC79 and the pure NiO nanowire, indicating a lower supercapacitive behavior, in good agreement with a specific capacitance derived from the charge/discharge measurement presented in Figure 8c. According to the plot of specific capacitance at 1 A g^{-1}, NGNC79 exhibits the highest capacitance of 628 F g^{-1} and graphene has the lowest capacitance of only 20.2 F g^{-1}. The specific capacitances of pure NiO and other composite structures at different NiO content (i.e., NGNC88, NGNC60 and NGNC43) are 425.6, 495.2, 444.3, and 368.5 F g^{-1}, respectively. NGNC79 is identified as the best sample with highest specific capacitance. Even though NGNC79 does not possess a highest surface area measured by BET (shown in a latter part), we postulate that it has electrochemically a highest active surface area and a strongest synergistic effect, providing more efficient electron transport. A higher amount of graphene in NGNC88 may block the active sites, resulting in a lower active surface area. It is interesting to notice that $NGNC79_{by\ mixing}$ possess capacitance of only 363.6 F g^{-1}, which is considerably lower than that of NiO. We speculate that graphene and NiO in $NGNC79_{by\ mixing}$ proportionally contribute to its specific capacitance without any synergistic effect. Moreover, the capacitance also mainly depends on the preparation process including weight measuring, mixing and drying, all of which are carefully prepared to ensure a good contact between the NiO nanowires and the graphene sheets. However, the good contact between the NiO nanostructure and the graphene matrix by mixing may not be achieved. On the other hand, NGNC79 prepared by the one-step sol−gel method followed by the calcination at the high temperature certainly results in improved contact between the NiO nanostructure and the graphene matrix.

dx.doi.org/10.1021/am500700x | ACS Appl. Mater. Interfaces 2014, 6, 8246−8256

Figure 9a demonstrates representative CV curves of nickel oxide/graphene nanocomposite with 79 wt % NiO (NGNC79) prepared by the sol−gel method at different scan rates. Carbon paper was used as a current collector to minimize the experimental errors and ensure accurate measurement of the intrinsic pseudocapacitive property. Oxidation peaks shift to higher and reduction peaks move toward lower potentials when the scan rate increases, leading to a larger potential separation between redox peaks. Figure 9b presents the galvanostatic charge/discharge curves in the potential ranges of 0−0.5 V at different current densities ranging from 1 to 15 A g^{-1}. On the basis of eq 1, the specific capacitance was calculated to be 628, 553, 486, 444, and 423 F g^{-1} at discharge current densities of 1, 2, 5, 10, and 15 A g^{-1}, respectively. As expected, it is observed that specific capacitance value (C_{sp}) decreases when scan rate increases. At a current density as high as 15 A g^{-1}, the NGNC 79 electrode can still retain 67.4% of its specific capacitance at a current of 1 A g^{-1}. The capacitance degradation has a more severe increasing at a higher charge/discharge current, which is largely due to the voltage drop commonly reported in many studies.[16,21,26] On the other hand, specific capacitance values of the electrode were also derived from the CV curves at different scan rates and shown in Table S1 (see the Supporting Information). The values are in good agreement with those from the charge/discharge curves.

Figure 9c depicts the Ragone plots (power density vs energy density) derived from charge/discharge curves of NGNC79 and NiO electrodes. The synergistic effect of the combination of the mesoporous NiO nanowire network and graphene sheets is clearly highlighted. The NGNC79 prepared by the one-pot sol−gel method followed by calcination can deliver a high energy of 21.8 W h kg^{-1} at a power density of 0.25 kW kg^{-1}, which is more than 1.5 times higher than that of NiO (14.7 W h kg^{-1}). At a higher power density of 7.5 kW kg^{-1}, the energy densities of NGNC79 and NiO electrodes are 12.7 and 8.7 W h kg^{-1}, respectively. Charge/discharge cycling was also carried out to investigate the electrochemical stability of the as-fabricated electrodes (NGNC79 and NiO) in a concentrated alkaline electrolyte. The results are shown in Figure 9d. The test was done for 3000 cycles in 6 M KOH at a discharge current of 1 A g^{-1} in potential windows of 0−0.5 V. Both the electrodes exhibit severe capacitance degradation in the first 300−500 cycles followed by gradual stabilization of specific capacitance from 1000th cycle onward. Upon completion of the test, NGNC79 and NiO retain 82.4% and 77.1% of their initial capacitances. There exists a slight improvement on the chemical stability of the NiO with the integration of graphene sheets in the nanowire network.

One of the major problems encountered with powdery samples is agglomeration that usually lowers active surface area. However, with the integration of graphene nanosheets as a supporting matrix for a nanowire network, we expected that the agglomeration problem could be minimized. Thus, BET measurements were performed on all samples and the results are shown in Figure 10 and Figure S7 in the Supporting Information. The results of the analysis are summarized in Table S2 (see the Supporting Information). NiO nanowire possesses a BET surface area of 81.6 m^2 g^{-1} and graphene has a surface area of 602 m^2 g^{-1}. The calculated surface area of graphene is much lower than its theoretical surface area (2630 m^2 g^{-1}),[18,27] which is largely due to disordered stacking and agglomeration of the graphene. On the other hand, all the NiO/graphene nanocomposites with any mass ratio have a larger surface area and bigger mean pore diameter than NiO, which is certainly advantageous to the transport of electrolytes and ionic diffusion during the charge/discharge process. NGNC79 and NGNC88 samples demonstrate the highest surface areas and largest pore diameters, implying excellent electrochemical properties. This is also consistent with the electrochemical evaluation conducted above.

As an attempt to understand the synergistic effect of the graphene incorporation into the composite electrode, electrochemical impedance spectroscopy (EIS) was also performed (Figure 11a, b). The equivalent circuit is shown in Figure S8

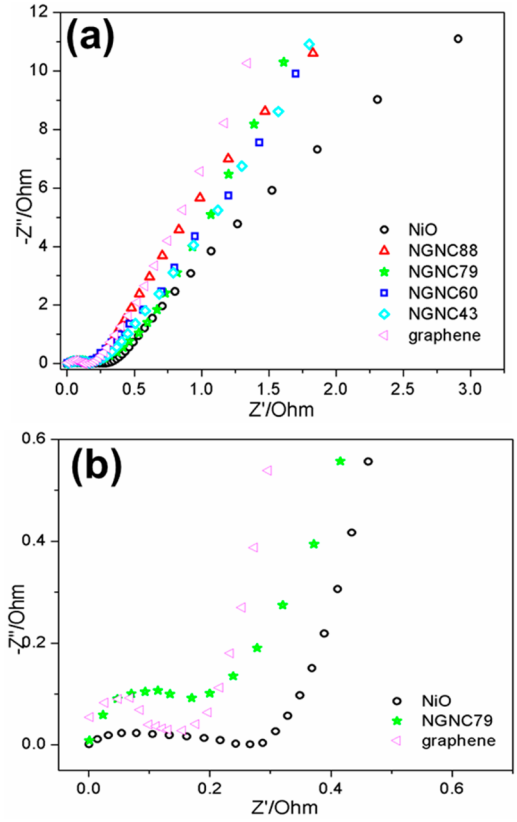

Figure 11. (a) Complex-plane impedance plots of NiO, NGNC88, NGNC79, NGNC60, NGNC43, and rGO electrodes. (b) Electrochemical impedance spectroscopy of NiO, NGNC79, and rGO electrodes in the high-frequency region.

(see the Supporting Information) and is similar to the circuit of graphene/metal oxide nanostructures reported in previous studies.[17,28,29] In complex plane plots, two distinct components can be clearly observed (i.e., the semicircular loop at high frequency and the linear segment at lower frequency), suggesting the presence of various electrochemical processes on the surface of the electrode. The former is attributed to the faradaic redox process, which is associated with surface properties of active materials. The semicircular loop is ascribed to the resistance at the metal oxide−electrolyte interface due to discontinuity in the charge transport at the solid oxide/liquid electrolyte interface. As such, its diameter can be utilized to estimate the charge transfer resistance of the electrode. The latter represents the diffusion of electrolyte species (OH^-) and its slope exhibits diffusive resistance of the electrolyte, or Warburg resistance presented in the electrical equivalent circuit. Among all samples, the graphene electrode has the smallest

dx.doi.org/10.1021/am500700x | ACS Appl. Mater. Interfaces 2014, 6, 8246−8256

diameter in high frequency ranges (0.1 Ω), while the pure NiO nanowire electrode exhibits the largest semicircular diameter (0.3 Ω). These other graphene/NiO nanocomposite materials have identical diameter/charge transfer resistance in the ranges of 0.15−0.17 Ω. This phenomenon was expected due to a high conductivity of graphene and the addition of graphene in the nanowire network would certainly significantly improve charge transfer. The direct adhesion of NiO on the graphene sheet enables fast electron transport, which in turn improves its pseudocapacitive behavior. Additionally, the slopes of the straight segments of the nanocomposite electrodes at different weight ratios were also higher than that of the pure NiO nanowire, indicating better ionic diffusion. The analysis results strongly demonstrate that the interaction between graphene and NiO, chemical stability and mechanical flexibility of graphene sheets prevent the agglomeration of NiO nanowires and primary nanoparticles.[30−32] In other words, it is possible to attribute improved capacitive properties of the composite to the advantageous combination of NiO nanowires and graphene sheets wherein the graphene acts as a highly conductive matrix.

CONCLUSIONS

In this paper, a facile technique was developed to prepare nanocomposite of graphene nanosheets and mesoporous NiO nanowires. The nanowires are composed of many primary nanoparticles evenly spaced from one another, forming a mesoporous structure. The nanowires were homogeneously distributed on graphene sheets with the aid of heat treatment in air, suggesting a tight interaction between them. Electrochemical measurements prove that the addition of graphene nanosheets as a flexible two-dimensional support for the nanowire network can result in a better pseudocapacitive behavior. On the basis of the analyses, the synergistic effect of the incorporation is responsible for a lowered internal resistance and an improved charge transfer. The integration of graphene can help in preventing the agglomeration of NiO nanowires, suggesting a higher surface area. The as-prepared NiO/graphene composite exhibits excellent supercapacitor properties: high specific capacitance, good cycle life and excellent rate capability. On top of that, this scalable strategy can be widely utilized to prepare other metal oxide/graphene composites for various applications, such as fuel cells, Li-ion batteries, and supercapacitors.

ASSOCIATED CONTENT

Supporting Information

Additional graphical representation of as-prepared nanostructures. This material is available free of charge via the Internet at http://pubs.acs.org/

AUTHOR INFORMATION

Corresponding Author

*E-mail: jmlee@ntu.edu.sg. Tel.:+65 651 381 29.

Notes

The authors declare no competing financial interest.

ACKNOWLEDGMENTS

This work is supported by Academic Research Fund (RGT27/13) of Ministry of Education in Singapore.

REFERENCES

(1) Conway, B. E. Transition from "Supercapacitor" to "Battery" Behavior in Electrochemical Energy Storage. *J. Electrochem. Soc.* **1991**, *138*, 1539−1548.
(2) Dam, D. T.; Nam, K.-D.; Song, H.; Wang, X.; Lee, J.-M. Partially Oxidized Titanium Carbonitride As A Non-noble Catalyst For Oxygen Reduction Reactions. *Int. J. Hydrogen Energy* **2012**, *37*, 15135−15139.
(3) Fan, Z. J.; Yan, J.; Wei, T.; Zhi, L. J.; Ning, G. Q.; Li, T. Y.; Wei, F. Asymmetric Supercapacitors Based on Graphene/MnO_2 and Activated Carbon Nanofiber Electrodes with High Power and Energy Density. *Adv. Funct. Mater.* **2011**, *21*, 2366−2375.
(4) Chen, Z.; Augustyn, V.; Wen, J.; Zhang, Y. W.; Shen, M. Q.; Dunn, B.; Lu, Y. F. High-Performance Supercapacitors Based on Intertwined CNT/V_2O_5 Nanowire Nanocomposites. *Adv. Mater.* **2011**, *23*, 791−795.
(5) Fang, Y. Z.; Jiang, F. T.; Liu, H.; Wu, X. M.; Lu, Y. Free-standing Ni-microfiber-supported Carbon Nanotube Aerogel Hybrid Electrodes In 3D For High-performance Supercapacitors. *R. Soc. Chem. Adv.* **2012**, *2*, 6562−6569.
(6) Wang, R. H.; Wang, Y.; Xu, C. H.; Sun, J.; Gao, L. Facile One-Step Hydrazine-Assisted Solvothermal Synthesis Of Nitrogen-doped Reduced Graphene Oxide: Reduction Effect and Mechanisms. *R. Soc. Chem. Adv.* **2013**, *3*, 1194−1200.
(7) Luo, Y. S.; Kong, D. Z.; Jia, Y. L.; Luo, J. S.; Lu, Y.; Zhang, D. Y.; Qiu, K. W.; Li, C. M.; Yu, T. Self-assembled Graphene@PANI Nanoworm Composites With Enhanced Supercapacitor Performance. *R. Soc. Chem. Adv.* **2013**, *3*, 5851−5859.
(8) Mao, S.; Pu, H. H.; Chen, J. H. Graphene Oxide And Its Reduction: Modeling And Experimental Progress. *R. Soc. Chem. Adv.* **2012**, *2*, 2643−2662.
(9) Dam, D. T.; Lee, J.-M. Capacitive Behavior Of Mesoporous Manganese Dioxide On Indium−tin Oxide Nanowires. *Nano Energy* **2013**, *2*, 933−942.
(10) Lu, Q.; Lattanzi, M. W.; Chen, Y.; Kou, X.; Li, W.; Fan, X.; Unruh, K. M.; Chen, J. G.; Xiao, J. Q. Supercapacitor Electrodes with High-Energy and Power Densities Prepared from Monolithic NiO/Ni Nanocomposites. *Angew. Chem., Int. Ed.* **2011**, *123*, 6979−6982.
(11) Shakir, I.; Shahid, M.; Cherevko, S.; Chung, C.-H.; K, D-.J. Ultrahigh-energy And Stable Supercapacitors Based On Intertwined Porous MoO_3−MWCNT Nanocomposites. *Electrochim. Acta* **2011**, *58*, 76−80.
(12) Shahid, M.; Liu, J.; Shakir, I.; Warsi, M. F.; Nadeem, M.; Kwon, Y.-U. Facile Approach To Synthesize $Ni(OH)_2$ Nanoflakes On MWCNTs For High Performance Electrochemical Supercapacitors. *Electrochim. Acta* **2012**, *85*, 243−247.
(13) Shakir, I.; Shahid, M.; Cherevko, S.; Chung, C.-H.; Kang, D. J. Ultrahigh-energy and stable supercapacitors based on intertwined porous MoO_3−MWCNT nanocomposites. *Electrochim. Acta* **2011**, *58*, 76−80.
(14) Hummers, W. S.; Offeman, R. E. Preparation of Graphitic Oxide. *J. Am. Chem. Soc.* **1958**, *80*, 1339−1339.
(15) Dam, D. T.; Wang, X.; Lee, J. M. Fabrication Of Mesoporous $Co(OH)_2$/ITO Nanowire Composite Electrode And Its Application In Supercapacitors. *R. Soc. Chem. Adv.* **2012**, *2*, 10512−10518.
(16) Dam, D. T.; Lee, J.-M. Ultrahigh Pseudocapacitance Of Mesoporous Ni-doped $Co(OH)_2$/ITO Nanowires. *Nano Energy* **2013**, *2*, 1186−1196.
(17) Wang, H.-W.; Hu, Z.-A.; Chang, Y.-Q.; Chen, Y.-L.; Lei, Z.-Q.; Zhang, Z.-Y.; Yang, Y.-Y. Facile Solvothermal Synthesis Of A Graphene Nanosheet−bismuth Oxide Composite And Its Electrochemical Characteristics. *Electrochim. Acta* **2010**, *55*, 8974−8980.
(18) Park, S. J.; Ruoff, R. S. Chemical Methods For The Production Of Graphenes. *Nat. Nanotechnol.* **2009**, *4*, 217−224.
(19) Frost, R. L.; Weier, M. L. Raman Spectroscopy Of Natural Oxalates At 298 And 77 K. *J. Raman Spectrosc.* **2003**, *34*, 776−785.
(20) Deabate, S.; Fourgeot, F.; Henn, F. X-ray Diffraction And Micro-Raman Spectroscopy Analysis Of New Nickel Hydroxide Obtained By Electrodialysis. *J. Power Sources* **2000**, *87*, 125−136.

(21) Dam, D. T.; Lee, J.-M. Polyvinylpyrrolidone-assisted Polyol Synthesis Of NiO Nanospheres Assembled From Mesoporous Ultrathin Nanosheets. *Electrochim. Acta* **2013**, *108*, 617−623.
(22) Yeo, B. S.; Bell, A. T. In Situ Raman Study of Nickel Oxide and Gold-Supported Nickel Oxide Catalysts for the Electrochemical Evolution of Oxygen. *J. Phys. Chem. C* **2012**, *116*, 8394−8400.
(23) Liu, R.; Duay, J.; Lee, S. B. Heterogeneous Nanostructured Electrode Materials For Electrochemical Energy Storage. *ChemComm* **2011**, *47*, 1384−1404.
(24) Wu, Z.-S.; Ren, W. C.; Wen, L.; Gao, L. B.; Zhao, J. P.; Chen, Z. P.; Zhou, G. M.; Li, F.; Cheng, H.-M. Graphene Anchored with Co_3O_4 Nanoparticles as Anode of Lithium Ion Batteries with Enhanced Reversible Capacity and Cyclic Performance. *ACS Nano* **2010**, *4*, 3187−3194.
(25) Yan, J.; Fan, Z. J.; Sun, W.; Ning, G. Q.; Wei, T.; Zhang, Q.; Zhang, R. F.; Zhi, L. J.; Wei, F. Advanced Asymmetric Supercapacitors Based on $Ni(OH)_2$/Graphene and Porous Graphene Electrodes with High Energy Density. *Adv. Funct. Mater.* **2012**, *22*, 2632−2641.
(26) Liu, R.; Lee, S. B. MnO_2/Poly(3,4-ethylenedioxythiophene) Coaxial Nanowires by One-Step Coelectrodeposition for Electrochemical Energy Storage. *J. Am. Chem. Soc.* **2008**, *130*, 2942−2943.
(27) Stoller, M. D.; Park, S. J.; Zhu, Y. W.; An, J. H.; Ruoff, R. S. Graphene-Based Ultracapacitors. *Nano Lett.* **2008**, *8*, 3498−3502.
(28) Fan, Z.; Yan, J.; Wei, T.; Zhi, L.; Ning, G.; Li, T.; Wei, F. Asymmetric Supercapacitors Based on Graphene/MnO_2 and Activated Carbon Nanofiber Electrodes with High Power and Energy Density. *Adv. Funct. Mater.* **2011**, *21*, 2366−2375.
(29) Yan, J.; Wei, T.; Qiao, W.; Shao, B.; Zhao, Q.; Zhang, L.; Fan, Z. Rapid Microwave-assisted Synthesis Of Graphene Nanosheet/Co_3O_4 Composite For Supercapacitors. *Electrochim. Acta* **2010**, *55*, 6973−6978.
(30) Ryu, I.; Yang, M.; Kwon, H.; Park, H. K.; Do, Y. R.; Lee, S. B.; Yim, S. Coaxial RuO_2−ITO Nanopillars for Transparent Supercapacitor Application. *Langmuir* **2014**, *30*, 1704−1709.
(31) Duay, J.; Gillette, E.; Hu, J.; Lee, S. B. Controlled Electrochemical Deposition And Transformation Of Hetero-nanoarchitectured Electrodes For Energy Storage. *Phys. Chem. Chem. Phys.* **2013**, *15*, 7976−7993.
(32) Lee, D. J.; Lee, H. K.; Song, J. C.; Ryou, M. H.; Lee, Y. M.; Kim, H. T.; Park, J. K. Composite Protective Layer For Li Metal Anode In High Performance Lithium-Oxygen Batteries. *Electrochem. Commun.* **2014**, *40*, 45−48.